



SPE 89867

Klinkenberg-Corrected Permeability Measurements in Tight Gas Sands: Steady-State Versus Unsteady-State Techniques

J.A. Rushing, SPE, Anadarko Petroleum Corp., K.E. Newsham, SPE, Apache Corp., P.M. Lasswell, OMNI Laboratories Inc., J.C. Cox, SPE, Texas Tech University, and T.A. Blasingame, SPE, Texas A&M University

Copyright 2004, Society of Petroleum Engineers Inc.

This paper was prepared for presentation at the SPE Annual Technical Conference and Exhibition held in Houston, Texas, U.S.A., 26–29 September 2004.

This paper was selected for presentation by an SPE Program Committee following review of information contained in a proposal submitted by the author(s). Contents of the paper, as presented, have not been reviewed by the Society of Petroleum Engineers and are subject to correction by the author(s). The material, as presented, does not necessarily reflect any position of the Society of Petroleum Engineers, its officers, or members. Papers presented at SPE meetings are subject to publication review by Editorial Committees of the Society of Petroleum Engineers. Electronic reproduction, distribution, or storage of any part of this paper for commercial purposes without the written consent of the Society of Petroleum Engineers is prohibited. Permission to reproduce in print is restricted to a proposal of not more than 300 words; illustrations may not be copied. The proposal must contain conspicuous acknowledgment of where and by whom the paper was presented. Write Librarian, SPE, P.O. Box 833836, Richardson, TX 75083-3836, U.S.A., fax 01-972-952-9435.

Abstract

This paper presents results from a laboratory study comparing Klinkenberg-corrected permeability measurements in tight gas sands using both a conventional steady-state technique and two commercially-available unsteady-state permeameters. We also investigated the effects of various rate and pressure testing conditions on steady-state flow measurements. Our study shows the unsteady-state technique consistently overestimates the steady-state permeabilities, even when the steady-state measurements are corrected for gas slippage and inertial effects. The differences are most significant for permeabilities less than about 0.01 md. We validated the steady-state Klinkenberg-corrected permeabilities with liquid permeabilities measured using both brine and kerosene. Although gas slippage effects are more pronounced with helium than with nitrogen, we also confirmed the steady-state results using two different gases. Moreover, we show results are similar for both constant backpressure and constant mass flow rate test conditions. Finally, our study illustrates the importance of using a finite backpressure to reduce non-Darcy flow effects, particularly for ultra low-permeability samples.

Introduction

Permeability measurements in core samples are based on the observation that, under steady-state flowing conditions, the pressure gradient is constant and is directly proportional to the fluid velocity. This constant of proportionality, as defined by Darcy’s law,

$$\frac{dp}{dx} = -\frac{\mu}{k} v_x \dots\dots\dots (1)$$

is the absolute core permeability, *k*. This relationship has been

validated for a wide range of flow velocities. For cores with permeabilities less than about 0.1 md, steady-state flow is difficult to achieve in a reasonable test time, especially when liquid is the flowing fluid. Consequently, gas is routinely used in low-permeability core samples. However, gas flow in tight gas sands is often affected by several phenomena that may cause deviations from Darcy’s law. Failure to account for these non-Darcy effects, principally gas slippage and inertial flow, may cause significant measurement errors.

Gas slippage is a non-Darcy effect associated with non-laminar gas flow in porous media. These effects occur when the size of the average rock pore throat radius approaches the size of the mean free path of the gas molecules, thus causing the velocity of individual gas molecules to accelerate or “slip” when contacting rock surfaces.¹ This phenomenon is especially significant in tight gas sands that are typically characterized by very small pore throats.

Klinkenberg,² who was one of the first to study and document gas slippage effects in porous media, showed the observed permeability to gas is a function of the mean core pressure. Furthermore, he observed that the gas permeability approaches a limiting value at an infinite mean pressure. This limiting permeability value, which is sometimes referred to as the equivalent liquid permeability¹ or the Klinkenberg-corrected permeability, is computed from the straight-line intercept on a plot of measured permeability against reciprocal mean pressure. In equation form, the line is defined by

$$k = k_{\infty} (1 + b/\bar{p}) \dots\dots\dots (2)$$

where *k*_∞ is the Klinkenberg-corrected permeability and *b* is the gas slippage factor. Experimental studies by Krutter and Day,³ Calhoun and Yuster⁴ and Heid, *et al.*,⁵ extended and validated the work of Klinkenberg.²

Inertial effects usually occur at high flow rates. These non-Darcy effects are a result of convective flow as fluid particles move through tortuous rock pore throats of varying sizes. Unlike steady-state Darcy flow, inertial effects are manifested by an increase in the pressure change without a corresponding or proportionate increase in fluid velocity. This additional pressure change is associated with dissipation of inertial energy as fluid particles accelerate through smaller pore throats and decelerate through larger areas. Furthermore, the fluid acceleration creates secondary flow patterns and an

irreversible conversion of kinetic energy to heat through viscous shear.^{6,7}

Early experimental research⁸⁻¹⁰ has documented inertial effects from gas flow in porous media and showed how the equation attributed to Forchheimer,¹¹

$$\frac{dp}{dx} = -\frac{\mu}{k}v_x + \beta\rho v_x^2 \dots\dots\dots (3)$$

is suitable for modeling these effects. Equation (3) indicates that, in single-phase fluid flow through a porous medium, both viscous and inertial forces counteract the externally applied force.¹² Note that inertial forces, as represented by the second term on the right side of Eq. (3) and quantified by the inertial resistance coefficient β , become more important as the fluid velocity increases. Conversely, viscous flow, which is modeled by the first term on the right side of Eq. (3), dominates when flow rates are low. In fact, Darcy’s equation is a special case of Forchheimer’s equation which reduces to Eq. (1) when inertial effects are negligible (*i.e.*, $\beta = 0$).

Because of long test times required to achieve steady-state flow in core samples with low permeabilities, most commercial laboratories use unsteady-state techniques to measure permeabilities in tight gas sands. Furthermore, the advent of efficient personal computers, high-speed data acquisition systems, and accurate pressure transducers has contributed to significant improvements in computer-controlled equipment that allows rapid and simultaneous measurement of Klinkenberg-corrected permeability, gas slippage factor, and the inertial resistance coefficient in tight gas sands.^{6,13-16} To solve for these three unknowns using essentially two equations, however, requires an iterative scheme which may introduce numerical errors. In addition, Ruth and Kenny¹⁷ have shown experimental errors may cause inaccurate measurements for certain ranges of permeability. Therefore, the primary objective of this paper is to investigate the accuracy of an unsteady-state technique for measuring Klinkenberg-corrected permeabilities in tight gas sands. We evaluate the accuracy of the unsteady-state permeameter by comparing results from a steady-state technique made under a variety of rate and pressure conditions.

Laboratory Program: Materials and Protocols

Test Materials. Permeability measurements were made on 26 core samples from wells producing in the Bossier tight gas sands in the Mimms Creek Field, Freestone County, TX. Effective sample porosity ranged from about 4% to 12%, while Klinkenberg-corrected permeability from the steady-state method (with no backpressure) ranged from about 0.0007 md to 0.10 md. Table 1 summarizes the intrinsic rock properties and core dimensions.

All permeability measurements represent absolute or specific values obtained at zero water saturation. Steady-state measurements were initially made using nitrogen, but were also repeated using helium on a subset of samples. All unsteady-state measurements were made with only helium as the flowing medium. Steady-state permeability measurements were also made on a subset of samples using liquid. Since the

Bossier sands are strongly water-wet, liquid permeabilities were initially measured using kerosene, but were also evaluated using brine, which was a synthetic fluid with a salinity of 50,000 ppm NaCl.

Table 1—Intrinsic Rock Properties and Core Dimensions

Sample No.	Core Length (cm)	Core Diameter (cm)	Effective Porosity (%)	Klinkenberg Permeability (md)
2-11	5.107	3.812	8.0	0.0011
2-12	3.261	3.807	6.4	0.00074
2-13	5.091	3.809	7.6	0.00096
2-14	3.516	3.818	5.8	0.0023
2-15	5.397	3.830	8.9	0.0022
2-33	3.868	3.805	8.0	0.0030
2-35	4.568	3.812	6.7	0.0013
2-54	5.055	3.795	7.3	0.0117
2-59	4.835	3.799	8.5	0.0380
2-71	4.949	3.806	8.4	0.0156
2-72	3.444	3.795	7.7	0.0057
4-1	4.025	3.799	7.9	0.0085
4-2	3.988	3.814	7.7	0.0032
4-9	4.439	3.795	8.1	0.0352
4-15	4.088	3.775	4.3	0.0008
4-18	4.620	3.788	9.9	0.0636
4-20	4.079	3.787	7.5	0.0098
4-22	4.315	3.796	10.1	0.0882
4-26	5.011	3.794	6.9	0.0061
4-48	4.675	3.745	11.3	0.0851
4-50	4.603	3.766	8.7	0.0161
4-51	4.525	3.765	11.0	0.0632
4-52	4.834	3.790	10.9	0.1150
5-33	3.377	3.772	10.0	0.0124
5-54	4.565	3.765	10.1	0.0188
5-55	4.077	3.778	12.6	0.0577

Laboratory Protocols. Steady-state measurements were made with a hydrostatic-type test cell. Backpressures were varied from atmospheric to about 200 psig, while the net overburden pressure was maintained at 800 psig relative to the mean core pressure for all measurements. Flow rates were measured using a bubble-tube flow meter, while upstream and downstream pressures were measured with pressure transducers.

Unsteady-state permeability measurements were made by two independent commercial laboratories using two different permeameters. Both unsteady-state permeameters, however, incorporate a pressure falloff technique⁶ where the downstream outlet port is vented to the atmosphere. Furthermore, the tests were conducted using helium as the flowing fluid. Note that, although the initial net overburden pressure was set at 800 psig, it varied both spatially and temporally during the unsteady-state measurements.

Prior to making any measurements, the cores were cleaned using a low-temperature azeotropic (chloroform-methanol) solution with a Dean Stark extraction process. The samples were then dried in a humidity-controlled environment. These cleaning and drying protocols were implemented to mitigate any damage or alteration of rock materials, especially the clays.

Diagnostic Tools to Evaluate Steady-State Flow

We evaluated the steady-state measurements using three different plotting techniques as diagnostic tools. First, we assessed gas slippage effects using the conventional

Klinkenberg plot,¹⁻⁵ *i.e.*, a plot of the inverse mean pressure against the apparent gas permeability. The Klinkenberg-corrected permeability is estimated from the y-intercept, while the gas slippage factor is computed from the line slope. As illustrated in the hypothetical Klinkenberg plot in Fig. 1, non-Darcy effects may be identified as deviations from the straight line trend at high mean pressures.

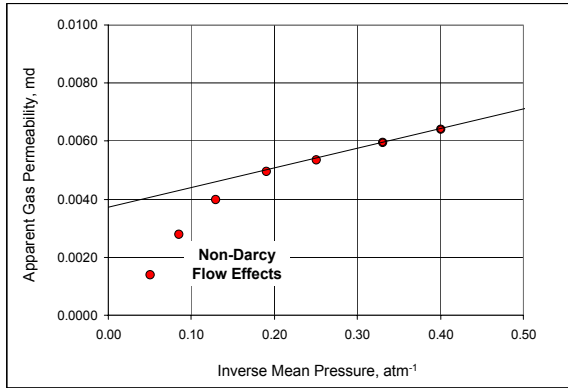


Fig. 1—Hypothetical Klinkenberg plot showing non-Darcy flow behavior identified as deviations from line at high mean pressures.

Note that the non-Darcy flow effects illustrated by Fig. 1 are often more evident in high-permeability samples.^{18,19} Consequently, we implemented a second diagnostic tool which is simply a plot of Darcy's equation for linear gas flow. As derived in Appendix A, a plot of the slippage-corrected Darcy pressure drop against mass flow rate should result in a line drawn through the origin with a slope equal to the inverse of Klinkenberg-corrected permeability.^{1,18,19} Non-Darcy flow effects, as shown by Fig. 2, are indicated by deviations upward from the line.

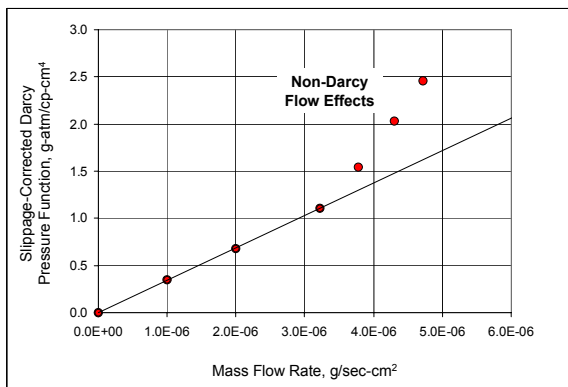


Fig. 2—Hypothetical slippage-corrected Darcy plot showing non-Darcy flow behavior identified as deviations from the line at high mass flow rates.

The third diagnostic tool was used to correct for inertial effects. Similar to Dranchuk and Kolada,¹⁸ we plot a slippage-corrected Forchheimer pressure change term against a slippage-corrected mass flow rate term. These plotting functions are derived in Appendix B. This plot, as illustrated in Fig. 3, should yield a line with a slope equal to the inertial resistance coefficient and an intercept equal to the inverse of Klinkenberg-corrected permeability.

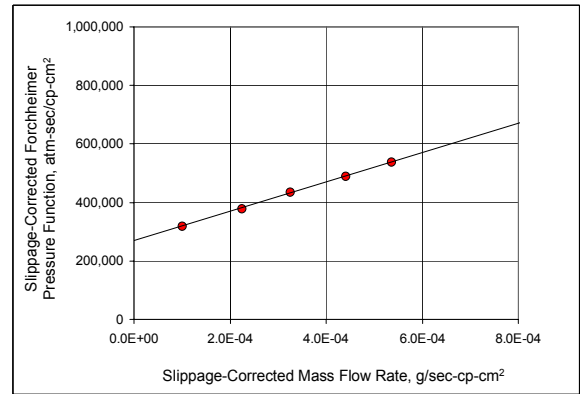


Fig. 3—Hypothetical slippage-corrected Forchheimer plot for computing Klinkenberg-corrected permeability and inertial resistance flow term.

Comparison of Unsteady-State and Steady-State Measurements with No Applied Backpressure

As noted, initial steady-state measurements for our study were made using nitrogen and with a backpressure equal to atmospheric pressure. We calculated Klinkenberg-corrected permeabilities and gas slippage factors using a plot of gas permeability against the inverse mean core pressure as suggested by Klinkenberg² and described by Eq. (2). Figure 4 is an example of a Klinkenberg plot for one of the core samples tested in our study.

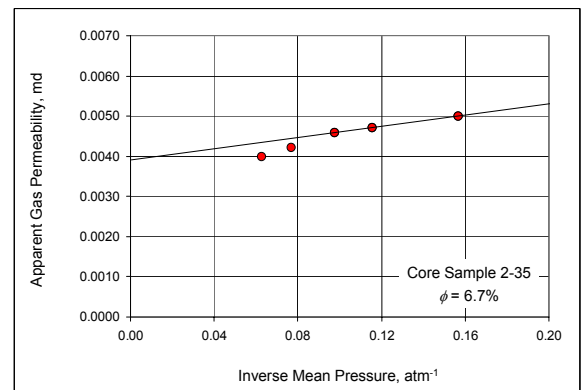


Fig. 4—Klinkenberg plot for Core Sample 2-35, zero backpressure.

Similar to observations made in References 18-20, we note that data points at higher mean pressures sometimes deviate downward from the best-fit line in Fig. 4. Since the Klinkenberg plot corrects for gas slippage effects, this deviation has been attributed to the onset of inertial effects and has been commonly described as visco-inertial flow.¹⁸ In general, the presence of visco-inertial flow is more evident in the lower permeability samples.

To compare with the steady-state results, we also employed two independent commercial laboratories to measure Klinkenberg-corrected permeabilities using an unsteady-state technique. Figure 5, which is a log-log plot comparing steady-state and unsteady-state results, indicates the unsteady-state technique overestimates the Klinkenberg-corrected permeability consistently over the entire range of permeabilities tested. The differences between unsteady-state

and steady-state techniques range from less than 5% for permeabilities greater than 0.02 md to more than 80% for a permeability less than about 0.01 md.

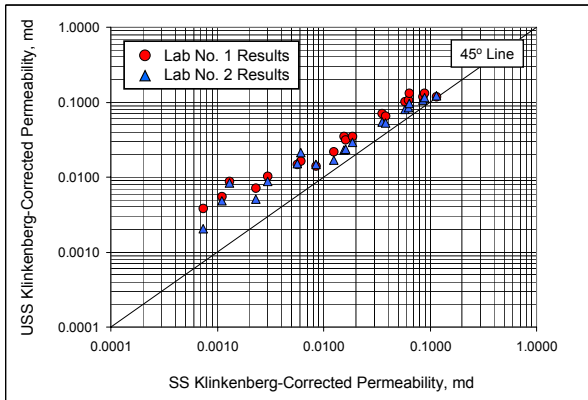


Fig. 5—Comparison of steady-state (SS) and unsteady-state (USS) Klinkenberg-corrected permeabilities.

Note also that, as indicated by Figure 6, the unsteady-state results from both laboratories are very similar. This similarity suggests the differences between unsteady-state and steady-state techniques may not be caused by simple random measurement errors, but are more likely a systematic phenomenon. Moreover, these errors may be attributed to fundamental problems with the unsteady-state methodology. On the basis of these observations, the next stages of our study focused on validating the steady-state results for a range of pressure and rate testing conditions.

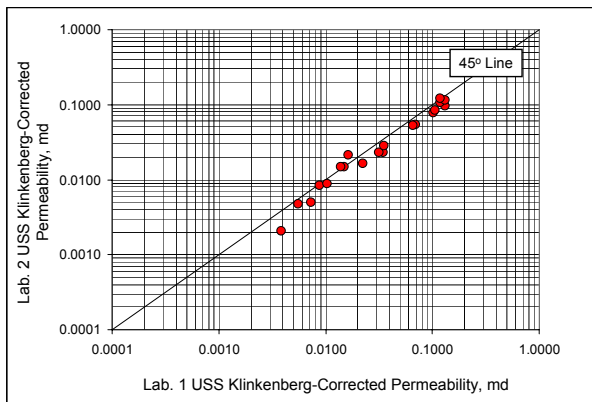


Fig. 6—Comparison of unsteady-state (USS) Klinkenberg-corrected permeabilities from two different commercial laboratories.

An Evaluation of Backpressure Effects on Steady-State Flow Measurements

McPhee and Arthur²⁰ suggest the use of a finite backpressure improves flow and pressure control. More importantly, application of a finite backpressure tends to minimize non-Darcy flow effects. To evaluate these effects, we measured Klinkenberg-corrected permeabilities for backpressures ranging from atmospheric to about 200 psig. Figure 7 illustrates the effects of backpressure on the Klinkenberg plot for backpressures of 0, 46.5, and 146.4 psig for core sample 2-35. Note that the Klinkenberg-corrected permeabilities at backpressures greater than zero exceed the value at zero backpressure by more than 10%.

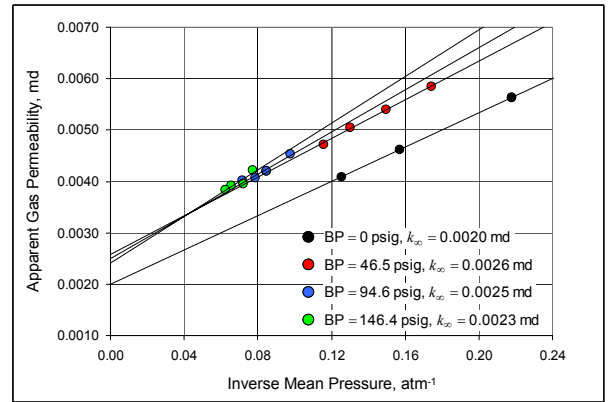


Fig. 7—Comparison of Klinkenberg plots at various backpressures (BP), Core Sample 2-35.

The effects of backpressure are more obvious if we present the steady-state data in a plot of slippage-corrected Darcy pressure drop against mass flow rate. Figures 8-10 are diagnostic plots of the slippage-corrected Darcy’s functions for core sample 2-35 and for backpressures of 0, 46.5, and 146.4 psig, respectively. Gas slippage factors were determined from Klinkenberg plots shown in Fig. 7. Similar to observations made in References 18-20, the presence of visco-inertial effects is indicated by data deviating upward from the line drawn through the origin. We also notice in Fig. 10 that these effects are reduced significantly at higher backpressures.

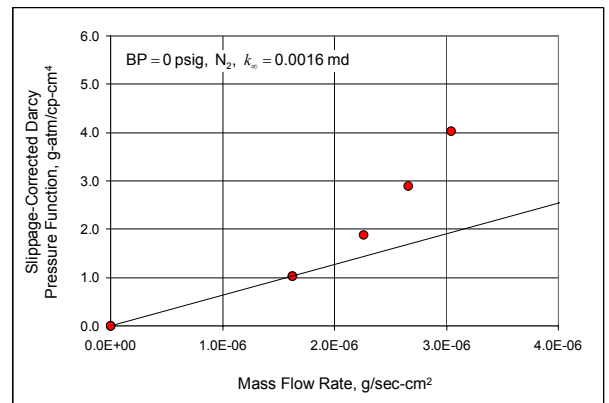


Fig. 8—Plot of slippage-corrected Darcy functions showing effects of backpressure, Core Sample 2-35, backpressure=0 psig.

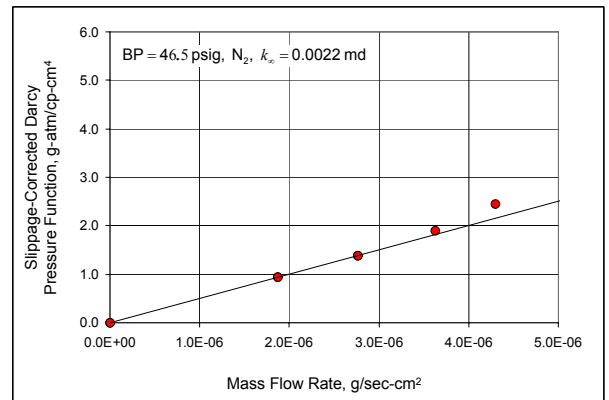


Fig. 9—Plot of slippage-corrected Darcy functions showing effects of backpressure, Core Sample 2-35, backpressure=46.5 psig.

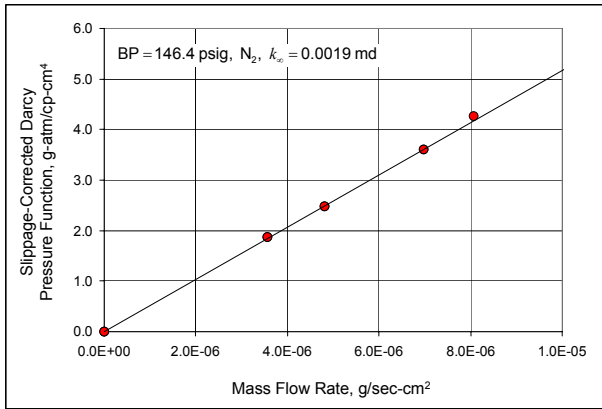


Fig. 10—Plot of slippage-corrected Darcy functions showing effects of backpressure, Core Sample 2-35, backpressure=146.4 psig.

To correct for the visco-inertial effects, we also employed a plot of the slippage-corrected Forchheimer pressure drop function against the slippage-corrected mass flow rate. The steady-state data shown in Figs. 9-10 are replotted in terms of the slippage-corrected Forchheimer functions in Figs. 11-12, respectively. Additionally, the same gas slippage factors used to compute the Darcy plotting functions were also used to generate the Forchheimer plotting functions. We note a reduction both in data scatter and line slopes as the backpressure is increased from 46.5 to 146.4 psig. Since the inertial resistance coefficient is related to the line slope, this change in slope suggests a reduction in non-Darcy flow effects as the backpressure is increased.

Klinkenberg-corrected permeabilities were calculated from the line properties in both the Darcy and Forchheimer plots. Figure 13 is a bar chart comparing these permeabilities from all of the diagnostic plots with that computed from the unsteady-state methods for core sample 2-35. Even when the steady-state measurements are corrected for gas slippage and inertial effects, the unsteady-state technique still overestimates the steady-state-derived permeabilities. For this example, the permeability derived from the unsteady-state technique is more than three times greater than those computed from steady-state methods. Again, the differences between the unsteady-state and corrected steady-state methods are greatest for permeabilities less than about 0.01 md.

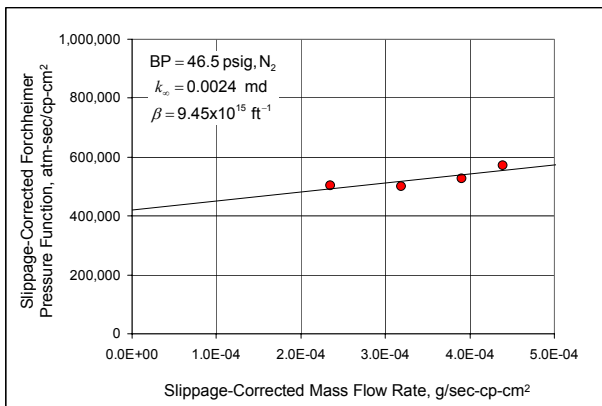


Fig. 11—Plot of slippage-corrected Forchheimer functions showing effects of backpressure, Core Sample 2-35, backpressure=46.5 psig.

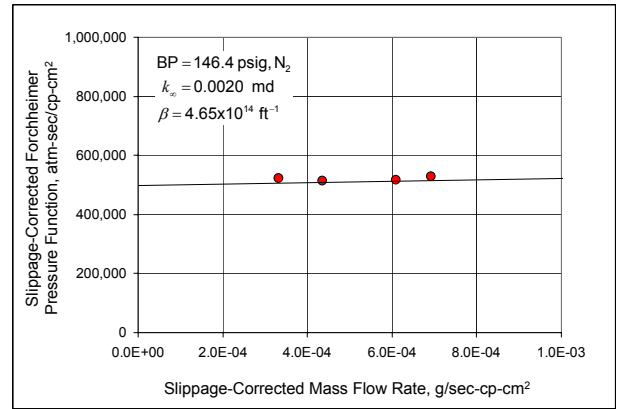


Fig. 12—Plot of slippage-corrected Forchheimer functions showing effects of backpressure, Core Sample 2-35, backpressure=146.4 psig.

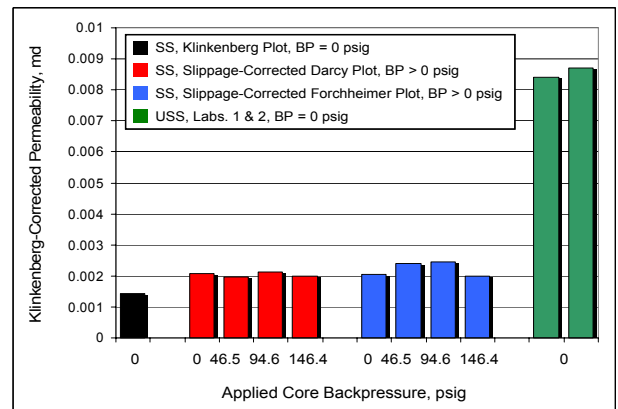


Fig. 13—Comparison of Klinkenberg-corrected permeabilities measured using steady-state (SS) and unsteady-state (USS) techniques and at various backpressures, Core Sample 2-35.

A Comparison of Steady-State Measurements: Helium vs. Nitrogen

The objective of the next phase of our investigation was to confirm the steady-state-derived Klinkenberg-corrected permeability measurements using a gas other than nitrogen. Since the unsteady-state permeameters used helium, we conducted an additional set of steady-state measurements using helium on a subset of core samples. These measurements removed any possible effects caused by the use of different gases, thereby allowing a more direct comparison between the unsteady-state and steady-state data. We also evaluated the effects of a finite backpressure on the permeability measurements with helium.

Figure 14 is a Klinkenberg plot for core sample 2-33 comparing steady-state measurements using helium and nitrogen at backpressures of 46 and 145 psig. We have also included for comparison the measurements made using nitrogen at a backpressure of zero. The data obtained with the helium have a greater slope and larger gas slippage factor, both of which are indicative of greater gas slippage effects than with nitrogen. When extrapolated back to an infinite mean pressure, both the helium and nitrogen data also converge to essentially the same intercept for both backpressures evaluated. We also observe that the Klinkenberg-corrected permeability obtained using nitrogen

with no backpressure is about 16% lower than all other measurements. We observed similar results for other core samples evaluated using both helium and nitrogen.

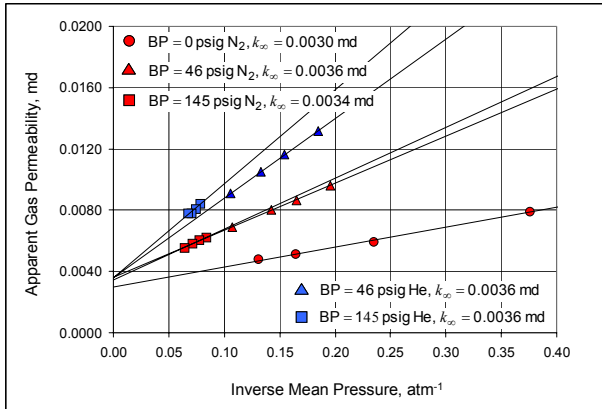


Fig. 14—Klinkenberg plot comparing steady-state (SS) measurements using helium and nitrogen at various backpressures (BP), Core Sample 2-33.

We also evaluated non-Darcy effects for the steady-state measurements made with helium. Figures 15 and 16 are plots of the slippage-corrected Darcy pressure function against mass flow rate for the helium data and at backpressures of 46 and 145 psig, respectively. Although some visco-inertial effects are seen at the lower backpressure, we observe that most non-Darcy effects have been reduced significantly for the range of flow rates investigated and for a backpressure of 145 psig. For comparison, we also show steady-state measurements using nitrogen for the same core sample. Figures 17 and 18 are plots of the slippage-corrected Darcy functions using the steady-state flow measurements made with nitrogen. Both sets of measurements illustrate the effectiveness of reducing non-Darcy flow effects with finite, higher backpressures.

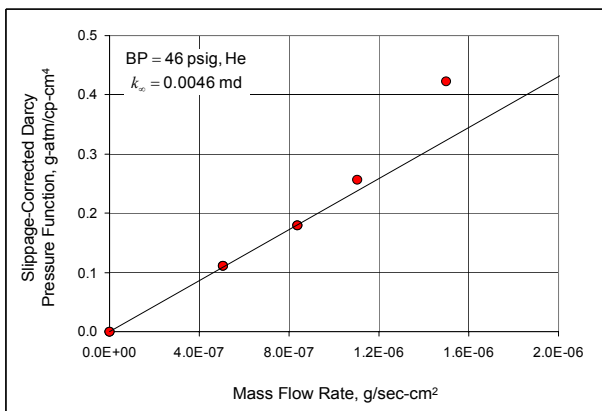


Fig. 15—Plot of slippage-corrected Darcy functions showing effects of backpressure on steady-state flow measurements using helium, Core Sample 2-33, backpressure=46 psig.

To correct for the visco-inertial effects, we again plotted the slippage-corrected Forchheimer pressure function against the slippage-corrected mass flow rate. Steady-state data shown in Figs. 15-18 are replotted in terms of the slippage-corrected Forchheimer functions in Figs. 19-22, respectively. The same gas slippage factors used to compute the Darcy plotting

functions in Figs. 15-18 were also used to generate the Forchheimer plotting functions. Again, we note a reduction in scatter for both helium and nitrogen as the backpressure is increased. We also observe a reduction in line slopes in Figs. 19-22 at higher backpressures. Since the inertial resistance coefficient (β) is related to the line slope, this change in slope reinforces the observation that we achieve a reduction in non-Darcy flow effects at higher backpressures.

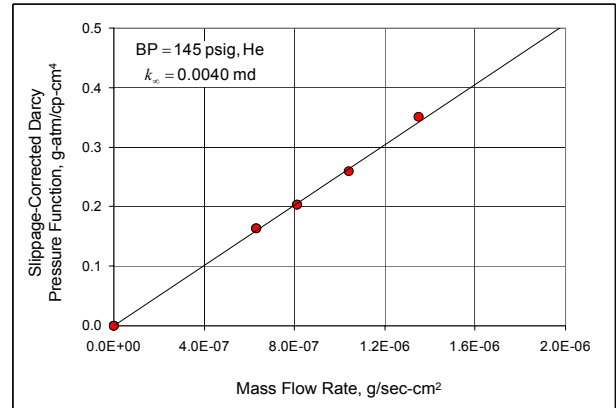


Fig. 16—Plot of slippage-corrected Darcy functions showing effects of backpressure on steady-state flow measurements using helium, Core Sample 2-33, backpressure=145 psig.

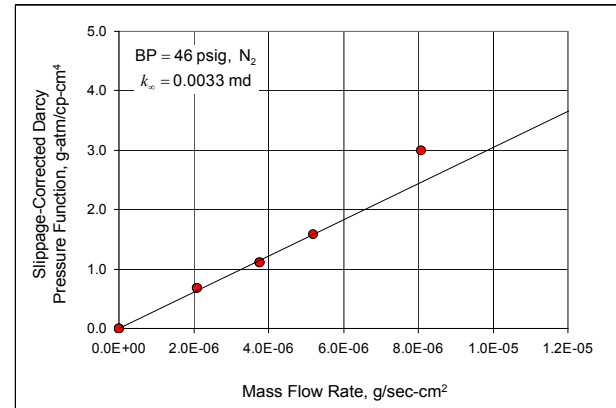


Fig. 17—Plot of slippage-corrected Darcy functions showing effects of backpressure on steady-state flow measurements using nitrogen, Core Sample 2-33, backpressure=46 psig.

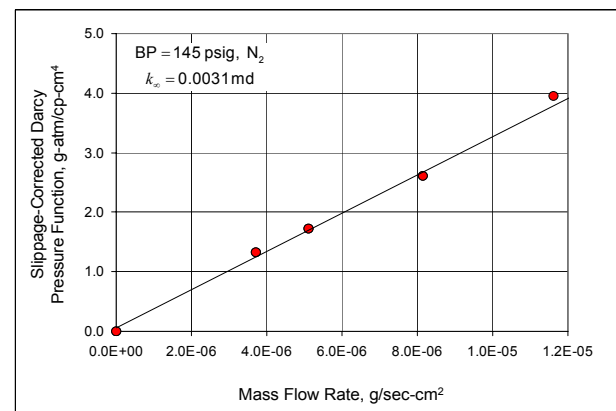


Fig. 18—Plot of slippage-corrected Darcy functions showing effects of backpressure on steady-state flow measurements using nitrogen, Core Sample 2-33, backpressure=145 psig.

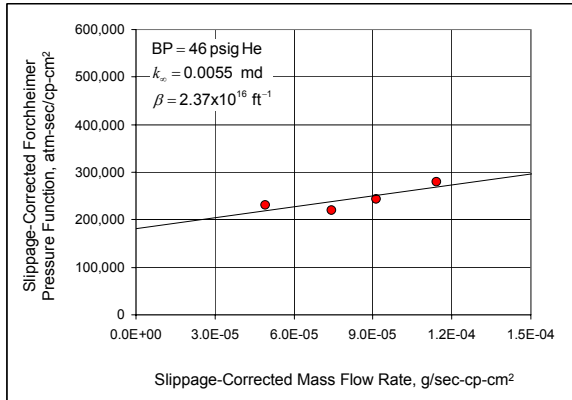


Fig. 19—Plot of slippage-corrected Forchheimer functions showing effects of backpressure on steady-state flow measurements using helium, Core Sample 2-33, backpressure=46 psig.

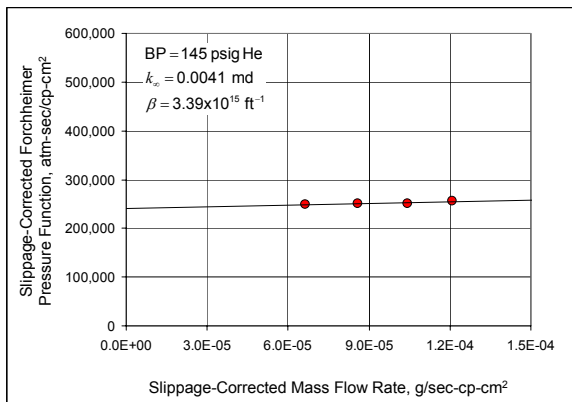


Fig. 20—Plot of slippage-corrected Forchheimer functions showing effects of backpressure on steady-state flow measurements using helium, Core Sample 2-33, backpressure=145 psig.

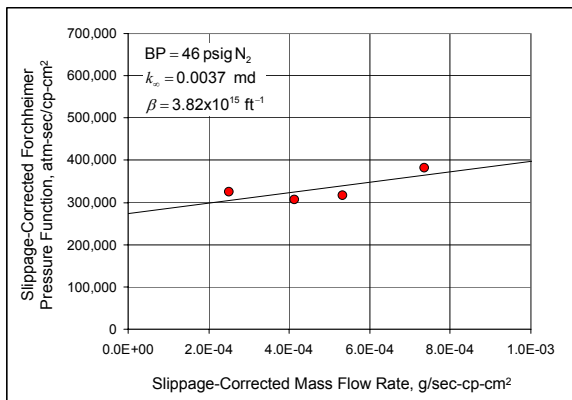


Fig. 21—Plot of slippage-corrected Forchheimer functions showing effects of backpressure on steady-state flow measurements using nitrogen, Core Sample 2-33, backpressure=46 psig.

As noted in Appendices A and B, the Klinkenberg-corrected permeability can be calculated from the line slope in Figs. 15-18 and from the line intercept in Figs. 19-22. Figure 23 is a bar chart comparing Klinkenberg-corrected permeabilities from the Darcy and Forchheimer diagnostic plots with that computed from the unsteady-state methods for core sample 2-33. We note again that, even when the steady-state

measurements are corrected for gas slippage and inertial effects, the unsteady-state technique still overestimates the steady-state-derived permeabilities. The permeability derived from the unsteady-state technique is more than two times greater than those computed from steady-state methods. We observed similar results for all core samples tested.

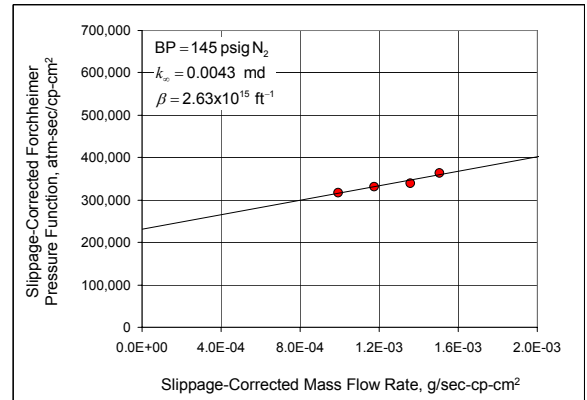


Fig. 22—Plot of slippage-corrected Forchheimer functions showing effects of backpressure on steady-state flow measurements using nitrogen, Core Sample 2-33, backpressure=145 psig.

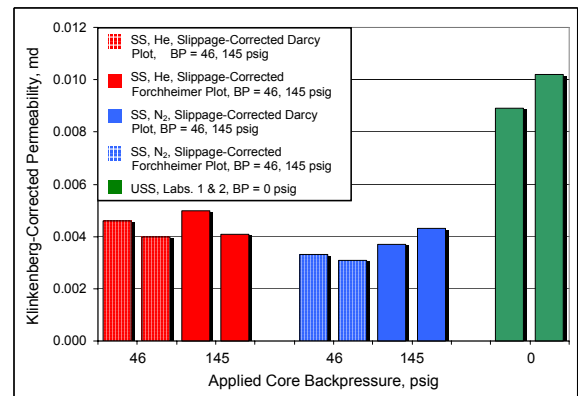


Fig. 23—Comparison of Klinkenberg-corrected permeabilities measured with steady-state (SS) and unsteady-state (USS) techniques using helium and nitrogen and at various backpressures, Core Sample 2-33.

Evaluation of Steady-State Measurements Under Constant Mass Flow Rate Conditions

McPhee and Arthur²⁰ also investigated the effects of various laboratory testing conditions on the accuracy of Klinkenberg-corrected permeabilities from steady-state flow measurements. Their study showed differences between the constant mass flow rate and constant pressure differential conditions were inconsequential when a finite backpressure was used. Most of the core samples evaluated in their study, however, had permeabilities significantly greater than 0.10 md. Therefore, the objective of this phase of our study was to evaluate the effects of constant mass flow rate conditions on steady-state measurements in ultra low-permeability samples.

Figures 24 and 25 are Klinkenberg plots for core sample 2-33 measured with constant mass flow rates of 4.0×10^{-6} and 8.0×10^{-6} g/sec-cm², respectively. Both steady-state measurements were made with nitrogen and at backpressures ranging from 50 to 150 psig. Although visco-inertial effects

are apparent in both plots, these non-Darcy effects appear to be more significant for the higher mass flow rate. The Klinkenberg-corrected permeabilities are, however, very similar for both mass flow rates. Furthermore, when compared to Klinkenberg-corrected permeabilities from steady-state measurements made under constant backpressure conditions (Fig. 23), we see the differences are negligible. We also note that the values obtained under constant mass flow conditions are still significantly lower than those estimated using the unsteady-state technique. Although not shown, we observed similar comparisons from other core samples tested.

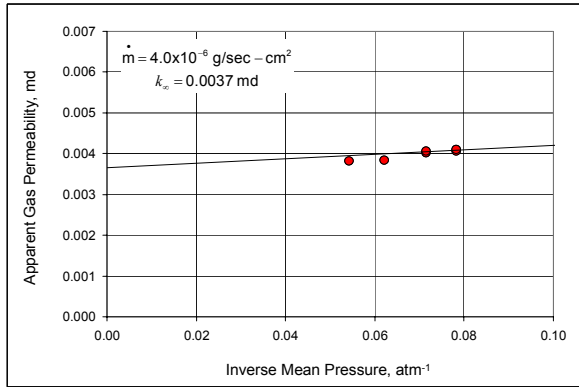


Fig. 24—Klinkenberg plot for core sample 2-33 showing steady-state measurements at a constant mass flow rate of 4.0×10^{-6} g/sec-cm².

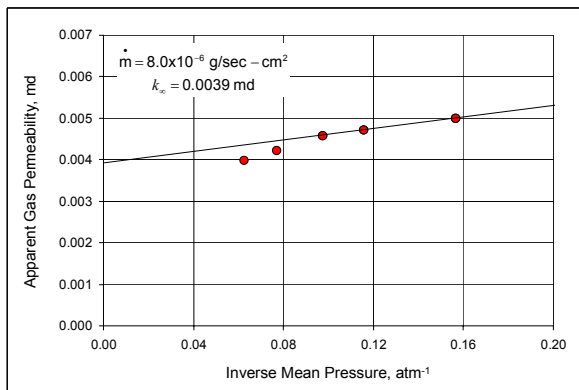


Fig. 25—Klinkenberg plot for core sample 2-33 showing steady-state measurements at a constant mass flow rate of 8.0×10^{-6} g/sec-cm².

Equivalent vs. Actual Liquid Permeabilities

The objective of the final phase of our study was to validate further the accuracy of the Klinkenberg-corrected permeabilities from the steady-state measurements. Recall that the Klinkenberg-corrected permeability estimated from the Klinkenberg plot is sometimes referred to as the equivalent liquid permeability. In fact, much of the initial laboratory research²⁻⁵ has established that “the absolute permeability of a porous medium to a non-reactive, homogeneous, single-phase liquid equals the equivalent liquid permeability.”¹ Consequently, we measured permeabilities to liquid on a subset of core samples representing a range of porosity and permeability.

Since the Bossier tight gas sands are strongly water-wet, we initially measured liquid permeabilities using kerosene in

order to mitigate any surface wetting effects. Figure 26 compares kerosene permeabilities to the Klinkenberg-corrected or equivalent liquid permeabilities for five core samples. The equivalent liquid permeabilities represent values obtained at a finite backpressure and corrected for both gas slippage and inertial effects using the slippage-corrected Forchheimer plotting technique. Note the excellent agreement between the kerosene permeabilities and the equivalent liquid or Klinkenberg-corrected permeabilities obtained using the steady-state method. We also see the liquid permeabilities are still lower than the Klinkenberg-corrected values estimated with the unsteady-state technique.

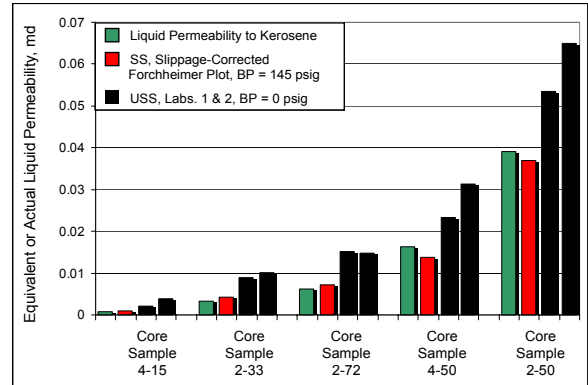


Fig. 26—Comparison of permeability to kerosene and equivalent liquid permeability for several core samples.

After cleaning and drying the kerosene-saturated core samples, we also measured permeabilities to brine, which is the wetting phase for the Bossier sands. As discussed in the section on laboratory protocol, the brine was a synthetic fluid with a salinity of 50,000 ppm NaCl. Figure 27, which is a comparison of brine permeabilities to the Klinkenberg-corrected or equivalent liquid permeabilities from the steady-state methods for the same five core samples, also shows excellent agreement. The equivalent liquid permeabilities again represent values obtained at a finite backpressure and corrected for both gas slippage and inertial effects using the slippage-corrected Forchheimer plotting technique. Similar to the comparison with kerosene permeabilities, we also see the permeabilities to brine are significantly lower than the values from the unsteady-state method.

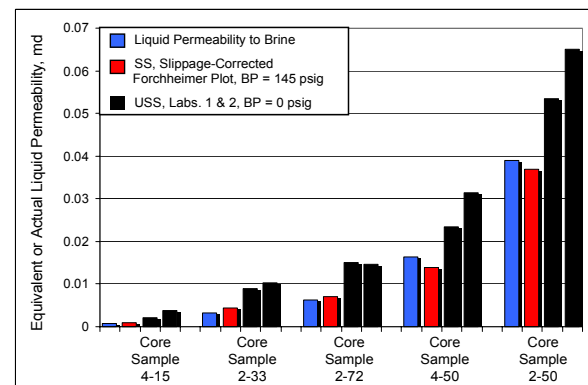


Fig. 27—Comparison of permeability to brine and equivalent liquid permeability for several core samples.

Tables 2 and 3 summarize results from Figs. 26 and 27, respectively, comparing equivalent liquid or Klinkenberg-corrected permeabilities from both the steady-state and unsteady-state techniques with actual liquid permeabilities measured with both kerosene and brine. Note that the Klinkenberg-corrected permeabilities were corrected for both gas slippage and inertial effects. Moreover, the excellent agreement observed between the steady-state equivalent liquid and the actual liquid permeabilities validates our steady-state gas measurements.

Table 2—Comparison of Equivalent and Kerosene Permeabilities for Various Core Samples

Core Sample No.	Klinkenberg-Corrected Permeability SS (md)	Kerosene Permeability (md)	Lab No. 1 Klinkenberg-Corrected Permeability USS (md)	Lab No. 2 Klinkenberg-Corrected Permeability USS (md)
4-15	0.0008	0.0007	0.0021	0.0038
2-33	0.0043	0.0033	0.0089	0.0102
2-72	0.0071	0.0062	0.0151	0.0147
4-50	0.0139	0.0163	0.0234	0.0314
2-59	0.0369	0.0390	0.0535	0.0650

Table 3—Comparison of Equivalent and Brine Permeabilities for Various Core Samples

Core Sample No.	Klinkenberg-Corrected Permeability SS (md)	Brine Permeability (md)	Lab No. 1 Klinkenberg-Corrected Permeability USS (md)	Lab No. 2 Klinkenberg-Corrected Permeability USS (md)
4-15	0.0008	0.0006	0.0021	0.0038
2-33	0.0043	0.0032	0.0089	0.0102
2-72	0.0071	0.0061	0.0151	0.0147
4-50	0.0139	0.0163	0.0234	0.0314
2-59	0.0369	0.0380	0.0535	0.0650

Summary and Conclusions

This paper presents results from a laboratory study comparing Klinkenberg-corrected permeability measurements in tight gas sands using both a conventional steady-state technique and two commercially-available unsteady-state permeameters. The primary study objective was to investigate the accuracy of the unsteady-state technique for applications in tight gas sands. We evaluated the accuracy of the unsteady-state permeameter by comparing results from a steady-state technique made under a variety of rate and pressure conditions. On the basis of our study, we offer the following conclusions:

1. Even when the steady-state measurements are corrected for gas slippage and inertial effects, the unsteady-state technique consistently overestimates Klinkenberg-corrected permeabilities. The differences range from less than 5% for permeabilities greater than 0.02 md to more than 80% for a permeability less than about 0.01 md.
2. The differences between measurement techniques are largest for steady-state measurements made with the downstream port venting to the atmosphere, *i.e.*, no backpressure. However, even when finite

backpressures are applied, we still observe errors in the unsteady-state measurements.

3. Permeabilities obtained from two independent commercial laboratories and using two different unsteady-state permeameters are very similar. This similarity suggests that the errors may not be caused by simple random measurement errors, but rather, such errors may be a systematic phenomenon that can be attributed to fundamental problems with the unsteady-state methodology. Further, these errors may be either mechanical, numerical, or both.
4. Equivalent liquid (*i.e.*, Klinkenberg-corrected) permeabilities obtained with a steady-state technique were validated with both brine and kerosene permeability measurements for a range of rock properties.
5. Steady-state measurements made with nitrogen were also confirmed using helium. Similar to observations made by other studies, gas slippage and inertial effects are more pronounced with helium than with nitrogen.
6. Use of a finite backpressure improves the accuracy of steady-state flow measurements, primarily by reducing both gas slippage and inertial effects. These non-Darcy effects are reduced by increasing the overall mean core pressure, thus causing the gas to behave more like a liquid.
7. We have also concluded that maintaining a constant mass flow rate will not materially affect the accuracy of steady-state flow measurements for the range of properties tested in our study.

Acknowledgments

We would like to express our thanks to the management of Anadarko Petroleum Corporation for their support and for permission to publish the results of our study. We would also like to thank OMNI Laboratories for their excellent work.

Nomenclature

- A = core cross-sectional area, cm²
 b = gas slippage factor, atm
 k = apparent permeability to gas measured at mean core pressure, md
 k_{∞} = Klinkenberg-corrected permeability, md
 L = core length, cm
 M = gas molecular weight, g/g-mole
 \dot{m} = mass flow rate = ρv_x , g/cm²-sec
 p_1 = upstream core pressure, atm
 p_2 = downstream core pressure, atm
 \bar{p} = average or arithmetic mean core pressure = $(p_1 + p_2)/2$, atm
 R = universal gas constant = 82.057 atm-cm³/g-mole °K
 T = absolute temperature, °K
 v_x = interstitial gas velocity in along core length, cm/sec

- \bar{z} = average gas deviation factor, dimensionless
- β = Forchheimer inertial resistance coefficient, cm^{-1}
- $\bar{\mu}$ = average gas viscosity, cp
- ρ = gas density, g/cm^3

Abbreviations

- BP = backpressure applied to core
- SS = steady-state flow conditions
- USS = unsteady-state flow conditions

References

1. Amyx, J.W., Bass, D.M., and Whiting, R.W.: *Petroleum Reservoir Engineering*, first edition, McGraw-Hill Publishing Co., New York, NY (1960), pp 91-93.
2. Klinkenberg, L.J.: "The Permeability of Porous Media to Liquids and Gases," paper presented at the API 11th Mid-Year Meeting, Tulsa, OK (May 1941); in *API Drilling and Production Practice* (1941) 200-213.
3. Krutter, H. and Day, R.J.: "Modification of Permeability Measurements," *Oil Weekly*, vol. 104, no. 4 (1941) 24-32.
4. Calhoun, J.C. and Yuster, S.T.: "A Study of the Flow of Homogeneous Fluids Through Ideal Porous Media," *API Drilling and Production Practice* (1946) 335-355.
5. Heid, J.G., et al.: "Study of the Permeability of Rocks to Homogeneous Fluids," *API Drilling and Production Practice* (1950) 230-246.
6. *Recommended Practices for Core Analysis*, Report RP 40, 2nd edition, Exploration and Production Dept., American Petroleum Institute, Washington, DC (Feb. 1998).
7. Katz, D.L., et al.: *Handbook of Natural Gas Engineering*, McGraw-Hill Publishing Co., New York, NY (1959), pp 46-51.
8. Fancher, G.H., et al.: "Some Physical Characteristics of Oil Sands," *Bull. 12*, Pennsylvania State C., Minerals Industries Experiment Station, University Park, PA (1933), 65.
9. Johnson, T.W. and Taliaferro, D.B.: "Flow of Air and Natural Gas Through Porous Media," *Technical Paper 592*, USBM (1938).
10. Green, L. and Duwez, P.: "Fluid Flow Through Porous Metals," *J. Applied Mech.* (Mar. 1951) 39-45.
11. Forchheimer, P.: "Wasserbewegung durch Boden," *Zeitz ver Deutsch Ing.* (1901) 48, 1731.
12. Geertsma, J.: "Estimating the Coefficient of Inertial Resistance in Fluid Flow Through Porous Media," *Soc. Pet. Engr. J.* (Oct. 1974), 445-450.
13. Jones, S.C., "A Rapid Accurate Unsteady-State Klinkenberg Permeameter," *Soc. Pet. Engr. J.* (Oct. 1972), 383-397.
14. Walls, J.D.: "Measurement of Fluid Salinity Effects on Tight Gas Sands with a Computer Controlled Permeameter," paper SPE 11092 presented at the 1982 SPE Annual Technical Conference and Exhibition, New Orleans, LA, Sept. 26-29.
15. Keelan, D.K.: "Automated Core Measurement System for Enhanced Core Data at Overburden Conditions," paper SPE 15185 presented at the 1986 SPE Rocky Mountain Regional Meeting, Billings, MT, May 19-21.
16. Jones, S.C., "A Technique for Faster Pulse-Decay Permeability Measurements in Tight Rocks," *SPE Formation Eval.* (Mar. 1997), 19-25.
17. Ruth, D.W. and Kenny, J.: "The Unsteady State Gas Permeameter," paper CIM 87-38-52 presented at the 1987 CIM Annual Technical Meeting of the Petroleum Society of CIM, Calgary, Alberta, Canada, June 7-10.

18. Dranchuk, P.M. and Kolada, L.J.: "Interpretation of Steady Linear Visco-Inertial Gas Flow Data," *J. Canadian Pet. Tech.* (Jan.-Mar. 1968) 36-40.
19. Noman, R. and Kalam, M.Z.: Transition from Laminar to Non-Darcy Flow of Gases in Porous Media, in *Advances in Core Evaluation: Accuracy and Precision in Reserves Estimation*, ed. P.F. Worthington (1990), pp 447-462.
20. McPhee, C.A. and Arthur, K.G.: Klinkenberg Permeability Measurements: Problems and Practical Solutions, in *Advances in Core Evaluation: Accuracy and Precision in Reserves Estimation*, ed. P.F. Worthington (1991), pp 447-462.
21. Morrison, S.J. and Duggan, T.P.: Non-Darcy Flow in Core Plugs: A Practical Approach, in *Advances in Core Evaluation: Accuracy and Precision in Reserves Estimation*, ed. P.F. Worthington (1991), pp 447-462.
22. Firoozabadi, A. and Katz, D.L.: "An Analysis of High-Velocity Gas Flow Through Porous Media," *J. Pet. Tech.* (Feb. 1979), 211-216.
23. Tek, M.R., Coats, K.H., and Katz, D.L.: "The Effect of Turbulence on Flow of Natural Gas Through Porous Reservoirs," *J. Pet. Tech.* (July 1962) 799-806.

Appendix A: Derivation of Plotting Functions for Diagnostic Plots Using Darcy's Equation^{1,18-20}

Beginning with Darcy's equation for linear, horizontal flow of a single-phase compressible fluid, the pressure gradient may be written as

$$\frac{dp}{dx} = -\frac{\bar{\mu}}{k} v_x \dots\dots\dots (A-1)$$

where gas viscosity is an average value at the mean core pressure and is assumed constant. Multiplying both sides by the fluid density, we obtain

$$\rho \frac{dp}{dx} = -\frac{\bar{\mu}}{k} \rho v_x \dots\dots\dots (A-2)$$

where ρv_x is the mass flow rate. Assuming a real gas, the gas density in terms of the real gas equation of state is

$$\rho = \frac{pM}{zRT} \dots\dots\dots (A-3)$$

where the gas deviation factor is also evaluated at the mean core pressure and is assumed constant. Substituting Eq. (A-3) into Eq. (A-2), we can rewrite Darcy's equation as

$$\frac{pM}{zRT} \frac{dp}{dx} = -\frac{\bar{\mu}}{k} \dot{m} \dots\dots\dots (A-4)$$

Separating variables and integrating gives

$$\frac{M}{zRT} \int_{p_1}^{p_2} p dp = -\dot{m} \frac{\bar{\mu}}{k} \int_0^L dx \dots\dots\dots (A-5)$$

Integrating Eq. (A-5) and rearranging terms yields

$$\frac{M(p_1^2 - p_2^2)}{2\bar{\mu}zRTL} = \frac{\dot{m}}{k} \dots\dots\dots (A-6)$$

Following the work of Dranchuk and Kolada, gas slippage effects² as defined by Klinkenberg’s equation

$$k = k_\infty(1 + b/\bar{p}) \dots\dots\dots (A-7)$$

can be included in Eq. (A-6) as follows:

$$\frac{M(p_1^2 - p_2^2)}{2\bar{\mu}zRTL} = \frac{\dot{m}}{k_\infty(1 + b/\bar{p})} \dots\dots\dots (A-8)$$

Rearranging terms yields

$$\frac{M(1 + b/\bar{p})(p_1^2 - p_2^2)}{2\bar{\mu}zRTL} = \frac{\dot{m}}{k_\infty} \dots\dots\dots (A-9)$$

The form of Eq. (A-9) suggests that a plot of the slippage-corrected Darcy pressure function against mass flow rate, *i.e.*,

$$\frac{M(1 + b/\bar{p})(p_1^2 - p_2^2)}{2\bar{\mu}zRTL} \text{ vs. } \dot{m}$$

will yield a line through the origin with a slope equal to the inverse of the Klinkenberg-corrected permeability. Note that the units of the slippage-corrected Darcy pressure function are g-atm/cp-cm⁴, while units of the mass flow rate term are g/sec-cm².

Appendix B: Derivation of Plotting Functions for Diagnostic Plots Using Forchheimer’s Equation^{7,18-20,23}

Similarly, the linear, horizontal flow of a single-phase compressible fluid written in terms of Forchheimer’s equation is

$$\frac{dp}{dx} = -\frac{\bar{\mu}}{k} v_x + \beta \rho v_x^2 \dots\dots\dots (B-1)$$

where gas viscosity is evaluated at the mean core pressure and is assumed constant. Multiplying both sides of Eq. (B-1) by fluid density yields

$$\rho \frac{dp}{dx} = -\frac{\bar{\mu}}{k} \rho v_x + \beta \rho^2 v_x^2 \dots\dots\dots (B-2)$$

where ρv_x is defined as the mass flow rate. Again, assuming a real gas defined by Eq. (A-3), Eq. (B-2) becomes

$$\frac{pM}{zRT} \frac{dp}{dx} = -\frac{\bar{\mu}}{k} \dot{m} + \beta \dot{m}^2 \dots\dots\dots (B-3)$$

Separating variables yields

$$\frac{M}{zRT} \int_{p_1}^{p_2} p dp = \left[-\frac{\bar{\mu}}{k} \dot{m} + \beta \dot{m}^2 \right] \int_0^L dx \dots\dots\dots (B-4)$$

Integrating Eq. (B-4) and rearranging terms gives

$$\frac{M(p_1^2 - p_2^2)}{2\bar{\mu}zRTL \dot{m}} = \frac{\beta}{\mu} \dot{m} + \frac{1}{k} \dots\dots\dots (B-5)$$

Similar to Eq. (A-9), we can incorporate gas slippage effects defined by Eq. (A-7) into Eq. (B-5) as follows:

$$\frac{M(p_1^2 - p_2^2)}{2\bar{\mu}zRTL \dot{m}} = \frac{\beta}{\mu} \dot{m} + \frac{1}{k_\infty(1 + b/\bar{p})} \dots\dots\dots (B-6)$$

Finally, if we rearrange terms, Eq. (B-6) becomes

$$\frac{M(1 + b/\bar{p})(p_1^2 - p_2^2)}{2\bar{\mu}zRTL \dot{m}} = \frac{\dot{m}(1 + b/\bar{p}) \beta}{\mu} + \frac{1}{k_\infty} \dots\dots\dots (B-6)$$

The form of Eq. (B-6) suggests a plot of the slippage-corrected Forchheimer pressure function against slippage-corrected mass flow rate, *i.e.*,

$$\frac{M(1 + b/\bar{p})(p_1^2 - p_2^2)}{2\bar{\mu}zRTL \dot{m}} \text{ vs. } \frac{\dot{m}(1 + b/\bar{p})}{\mu}$$

will yield a line with a slope equal to the inertial resistance coefficient and an intercept equal to the inverse of Klinkenberg-corrected permeability. Note that the units of the slippage-corrected Forchheimer pressure function are atm-sec/cp-cm², while units of the mass flow rate term are g/sec-cp-cm².